Development and validation of a fast thermal finite element solver

M. Schöning, E. Lange and K. Hameyer
Institute of Electrical Machines, RWTH Aachen University,
Schinkelstr. 4, D-52056 Aachen, Germany
phone: (+49)-241-80-97667, fax: (+49)-241-80-92270
E-mail: Marc.Schoening@iem.rwth-aachen.de

***Abstract*—Nowadays, the knowledge of temperatures inside electrical machines is an important criteria, especially if further power density enhancements or frame size reductions are aimed at. Furthermore, temperature estimation in permanent magnets is an essential part of the design process for electrical machine due to their affect on the electromagnetic behaviour. In this paper a particularly fast thermal finite element solver is introduced. By use of boundary conditions for thin layer geometries and the air gap, the number of elements can be reduced significantly.**

I. Introduction

INCREASING requirements on power density and reduced frame sizes lead to new challenges in the design process of electrical machines. In particular, the estimation of temperatures and heat flow inside electrical machines, especially for permanent magnet synchronous machines is of main interest. There are various approaches available using the lumped parameter technique [1], [2], [3] allowing for a fast prediction of temperatures in prior defined positions. The calculation is performed by defining a thermal network of the specific machine, where the machine geometry is described by thermal resistances and the available losses are regarded as heat sources. An obvious limitation is, that the lumped parameter model requires an intensive adaptation for each new machine by parametrizing the thermal resistances through prototype measurements. Alternatively, a knowledge database from prior machine designs can be used to adapt the lumped parameter model. Another approach is to use available software packages for a finite element simulation of the thermal behaviour of the device under study. In this case, the thin slot insulation between stator lamination and copper must be modelled leading to a huge number of elements, which results in high computational costs. In addition, the heat transfer in the air gap has to be regarded. This can be achieved by a coupled fluid dynamics analysis which also will lead to a long computational time. In this paper, a finite element solver is introduced regarding slot insulations and the air gap by the use of boundary conditions. This approach reduces the number of elements significantly. Furthermore, a thermal measurement is accomplished, to validate and adapt the parameters used for the boundary conditions.

II. Boundary Conditions

For the thermal simulation of electrical machines, several boundary conditions must be introduced. They can be divided in two categories:

- physically motivated boundary conditions.
- model motivated boundary conditions, required due to the modeling with finite elements.

Natural boundary conditions include convection, radiation and defined temperature profiles. Artificial boundary conditions consist of thin thermal transition layers and fluid gaps.

A. Convection

Assuming a heat flow proportional to the temperature difference between solid and enclosing fluid, the convective heat transfer can be modelled by the *Robin*- or *Cauchy* boundary condition defined as:

$$-\lambda \nabla T = h(T - T_\infty). \tag{1}$$

The temperature T_∞ as well as the heat transfer coefficient h need to be known. h depends on the surface property of the solid, the temperature and the form of the flow (turbulent or laminar).

B. Radiation

For the radiation, the heat flow is proportional to the temperature difference to the power of four. The mathematical expression of the radiation is:

$$-\lambda \nabla T = k_b \varepsilon (T^4 - T_\infty^4). \tag{2}$$

By applying the third binomial formula, the following substitution can be made:

$$h_r := k_b \varepsilon (T^2 + T_\infty^2)(T + T_\infty). \tag{3}$$

h_r is a non-linear heat transfer coefficient including the Boltzmann constant k_b and the emissivity ε. Due to the mathematical transformation, the radiation can be expressed by the Robin boundary condition [4]:

$$-\lambda \nabla T = h_r (T - T_\infty).$$

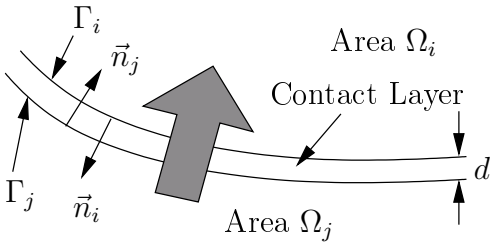

Figure 1. Thin layer boundary condition.

C. Thin Layer

For the slot isolation in electrical machines, the approach introduced in [5] is applied. Describing thin material layers by a boundary condition, the number of required elements can be reduced significantly. As indicated in fig. 1, a heat exchange occurs between area Ω_i and Ω_j. Assuming, that the thickness d is small compared to the other dimensions, the heat flow is perpendicular to the contact layer and can be conveyed by a thermal resistance [6]:

$$R_{th} = \frac{1}{h_k A}. \tag{4}$$

With a known thermal conductivity λ_k of the insulation material, the resistance coefficient h_k can be determined:

$$R_{th} = \frac{d}{\lambda_k A} = \frac{1}{\frac{\lambda_k}{d} A} \Rightarrow h_k = \frac{\lambda_k}{d}. \tag{5}$$

Therewith, the boundary conditions for Γ_i and Γ_j are defined as:

$$-\lambda_i \nabla T_i = h_k (T_i - T_j), \tag{6}$$
$$-\lambda_j \nabla T_j = h_k (T_j - T_i), \tag{7}$$

D. Air gap

To represent the air gap of a rotating machine, the Taylor [7] mechanism is assumed. This physical model is examined in [8], [9], [10] and still used for the nowadays design of electrical machines in the absence of forced axial flow [11]. By neglecting the slot form and other roughness of rotating cylinders, a dimensionless coefficient (nusselt number) can be determined [9]:

$$Nu = 2 \qquad for\ \frac{T_a}{F_g} < 1700$$
$$Nu = 0.128 \left(\frac{T_a}{F_g}\right)^{0.367} \qquad for\ 1700 < \frac{T_a}{F_g} < 10^5$$
$$Nu = 0.409 \left(\frac{T_a}{F_g}\right)^{0.241} \qquad for\ 10^5 < \frac{T_a}{F_g} < 10^7.$$

The modified *Taylor* number $\frac{Ta}{F_g}$ is in indicator for turbulences (s. Fig. 2). T_a is defined as:

$$T_a = \frac{\rho^2 \omega^2 r_m b^3}{\mu^2} \tag{8}$$

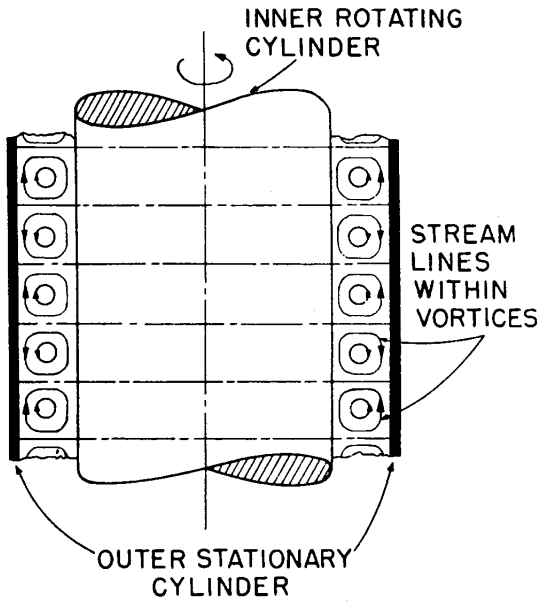

Figure 2. Rotating Taylor turbulences [8].

where ρ describes the density of air, ω the angular velocity, r_m the middle air gap radius, b the air gap height and μ the viscosity of the air. The geometrical correction factor F_g reads:

$$F_g = \frac{\pi^4}{1697(1-\frac{b}{2r_m})^2 \left[\frac{0{,}00056+0{,}0571(\frac{2r_m-2{,}304b}{2r_m-b})^2}{(\frac{2r_m-2{,}304b}{2r_m-b})^2}\right]}. \tag{9}$$

Assuming, that there is no heat flow in axial direction and with $Nu = \frac{2h_c b}{\lambda_{air}}$, the boundary conditions can be expressed as:

$$-\lambda_r \nabla T_r = h_c (T_r - \overline{T}_s) \qquad stator\ surface$$
$$-\lambda_s \nabla T_s = h_c (T_s - \overline{T}_r) \qquad rotor\ surface$$

$\overline{T}_s$ and $\overline{T}_r$ represent the mean temperatures in the stator and the rotor. Therewith, the required boundary conditions for thermal simulations of electrical machines are defined.

III. System Matrix

The general system of equations for one element Ω_i is defined as:

$$(\mathbf{S}_1 + \mathbf{S}_2)\vartheta + \mathbf{M}\dot{\vartheta} = \mathbf{B}, \tag{10}$$

where ϑ is a vector representing the temperature in every node.

Furthermore, the following definitions are applied:

$$\Xi = [\xi_1, \xi_2, \ldots, \xi_p],$$

$$N = \begin{bmatrix} \frac{\partial \xi_1}{\partial x} & \frac{\partial \xi_2}{\partial x} & \cdots & \frac{\partial \xi_p}{\partial x} \\ \frac{\partial \xi_1}{\partial y} & \frac{\partial \xi_2}{\partial y} & \cdots & \frac{\partial \xi_p}{\partial y} \\ \frac{\partial \xi_1}{\partial z} & \frac{\partial \xi_2}{\partial z} & \cdots & \frac{\partial \xi_p}{\partial z} \end{bmatrix}.$$

ξ are the element shape functions. The first part of the element stiffness matrix $\mathbf{S}_1$ reads:

$$\mathbf{S}_1 = \int_{\Omega_i} \lambda N^T N \, \mathrm{d}\Omega.$$

The second part of the element stiffness matrix $\mathbf{S}_2$ yields:

$$\mathbf{S}_2 = \int_{\Gamma_i} h \, \Xi^T \Xi \, \mathrm{d}\Gamma.$$

For a transient simulation, the mass matrix $\mathbf{M}$ is taken into account:

$$\mathbf{M} = \int_{\Omega_i} \rho c \Xi^T \Xi \, \mathrm{d}\Omega.$$

The load vector $\mathbf{B}$ consists of the heat sources $\dot{q}$, the heat flow q and the surrounding temperature T_∞ of the Robin Boundary condition:

$$\mathbf{B}_1 = \int_{\Omega_i} \dot{q} \, \Xi^T \, \mathrm{d}\Omega,$$

$$\mathbf{B}_2 = \int_{\Gamma_i} q \, \Xi^T \, \mathrm{d}\Gamma,$$

$$\mathbf{B}_3 = \int_{\Gamma_i} h T_\infty \, \Xi^T \, \mathrm{d}\Gamma,$$

In summary, the load vector $\mathbf{B}$ is defined as:

$$\mathbf{B} = \mathbf{B}_1 + \mathbf{B}_2 + \mathbf{B}_3.$$

For solving the system of equation and to regard non-linearities as well as the time dependency, the Newton-Raphson and Euler methods [12] are applied.

IV. Validation

First, the model motivated boundary conditions, taking the slot insulation and the air gap into account, are verified. Afterwards, an induction machine is measured and simulated and the results are compared.

A. Thin layer boundary condition

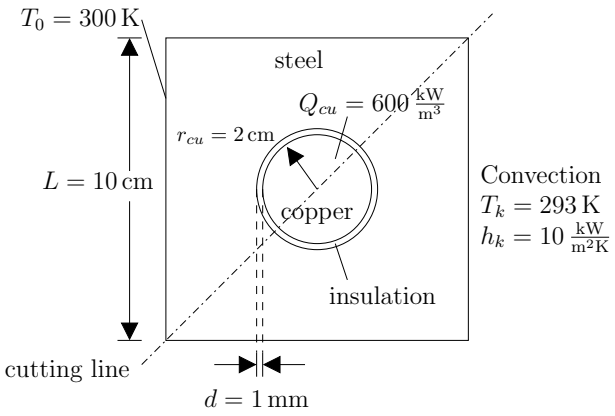

Figure 3. Copper bar embedded in steel.

To verify the thin layer boundary condition (q. v. II-C), a two-dimensional geometry is introduced, representing a copper bar embedded in steel (s. Fig. 3). An insulation material is placed between the copper and the steel. For the verification, two finite element models are built, one using the boundary condition for thin layers, the second with a modelled insulation (s. Fig. 4). To compare the simulation results of both models, the temperature along the cutting line is plotted (s. Fig. 5). The relative deviation is illustrated in a logarithmic scale. If the insulation is modeled by the boundary condition, the deviation increases around the insulation, because of the discontinuity between copper and steel. It can be confirmed, that thin layer boundary conditions can be applied, if the temperature inside the insulation is of no interest. Thereby, the number of elements can be reduced significantly resulting in a time optimized simulation.

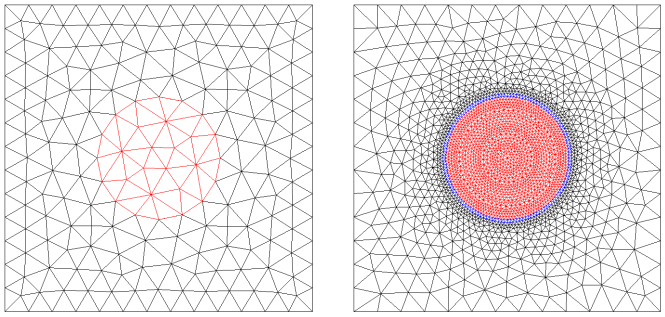

(a) W/o insulation (354 elements). (b) With insulation (4870 elements).

Figure 4. Used finite element models.

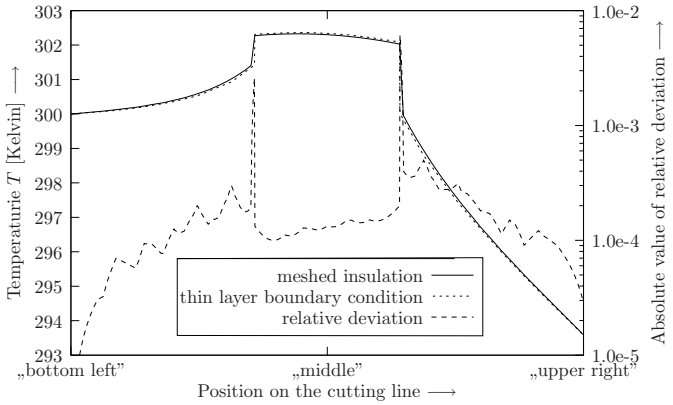

Figure 5. Comparison of the calculated temperatures on the cutting line.

B. Air gap

The implemented boundary condition (q. v. II-D) regarding the air gap of electrical machines is verified by a test arrangement, illustrated in Fig. 6. It consists of two solids, separated by a gap of thickness d. The gap represents a fluid with the thermal conductivity λ_f. For this test arrangement, two models are created, one with a discretized fluid, the other one using the artificial boundary condition. The relation between the thermal conductivity λ_f of the modelled fluid and the equivalent heat flow coefficient h_f of the boundary condition is given by:

$$h_f = \frac{\lambda_f}{d}. \tag{11}$$

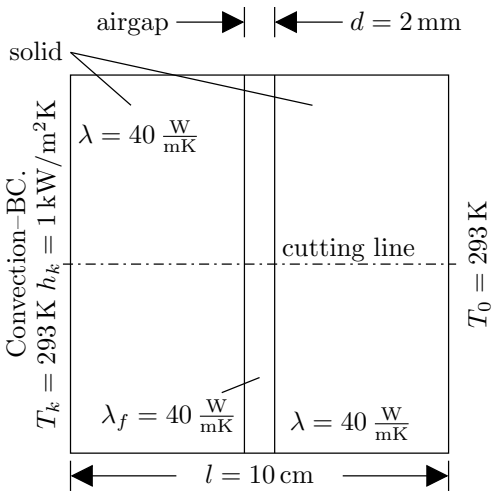

Figure 6. Test arrangement to verify the air gap boundary condition.

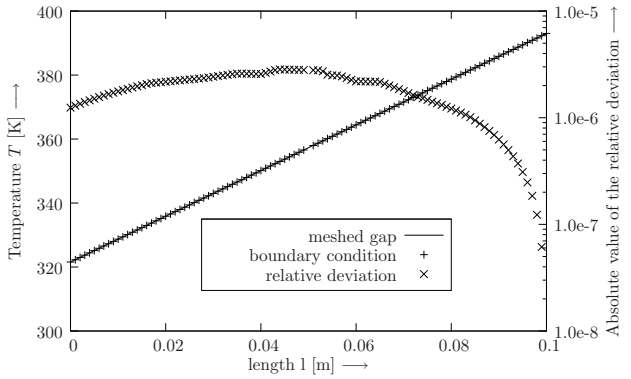

Figure 7. Temperature distribution on the cutting line of the test arrangement.

The simulation result is shown in Fig. 7. As expected, a continuous temperature distribution along the cutting line is calculated, showing a well agreement of the modelled fluid gap and the boundary condition. In Fig. 8, the result around the air gap is pointed out. Inside the air gap, the relative deviation is 1, because of using the boundary condition. This means, that the temperature in the air gap is not calculated. Outside the air gap, the relative deviation is 10^{-6}. Therefore, both modelling approaches achieve equivalent results. The advantage of using

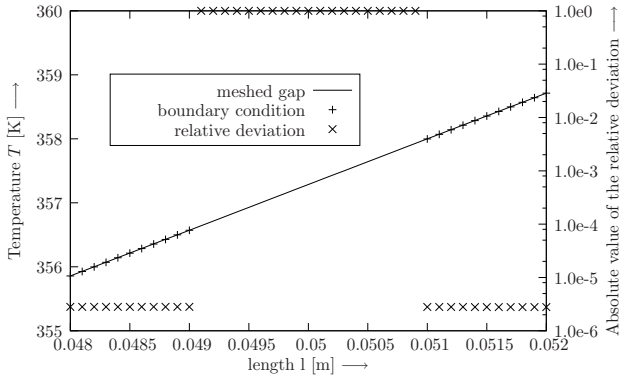

Figure 8. Temperature distribution on the cutting line near the air gap.

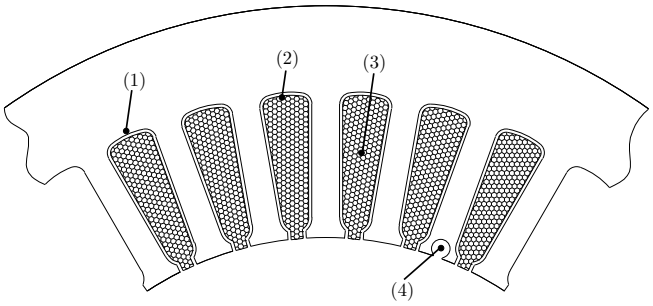

Figure 9. Position of the thermal sensors in the stator.

the boundary condition is a significant reduction of necessary finite elements and a reduced computation time.

C. Induction machine

For the validation and parametrization of the presented solver, an induction machine is measured. As illustrated in figure 9, thermal sensors are placed in the stator teeth (pos. 4), the copper windings (pos. 3), between slot insulation and copper (pos. 2) and between stator sheet and slot insulation (pos. 1). Furthermore, thermal sensors are attached to the rotor surface. To transfer the data from the rotating measuring points on the rotor surface, data loggers, equipped with infrared ports, are used (see fig. 10). Additionally, the ambient temperatures above and below the machine are detected as well as the frame temperature, which is observed by a thermal imaging camera. The experimental setup of the induction machine is illustrated in fig. 11. For the numeric simulation, a two-dimensional finite element model is used, discretized by 12150 elements. The computation on a 2 Ghz Processor is completed in 10 seconds. The calculated and measured temperatures (in ^{o} Celsius, ambient temperature 26^oC) are listed in table I, whereas the

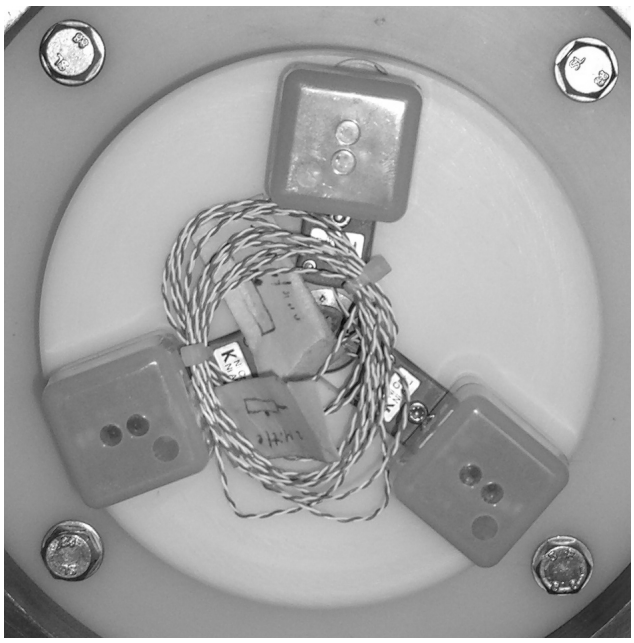

Figure 10. Data loggers attached to the rotor.

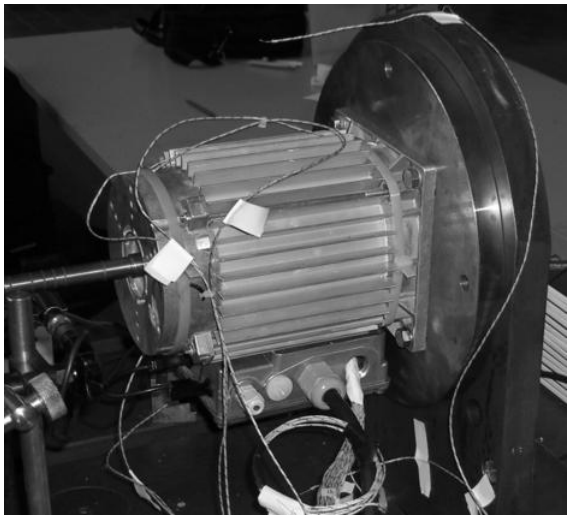

Figure 11. Experimental measurement setup.

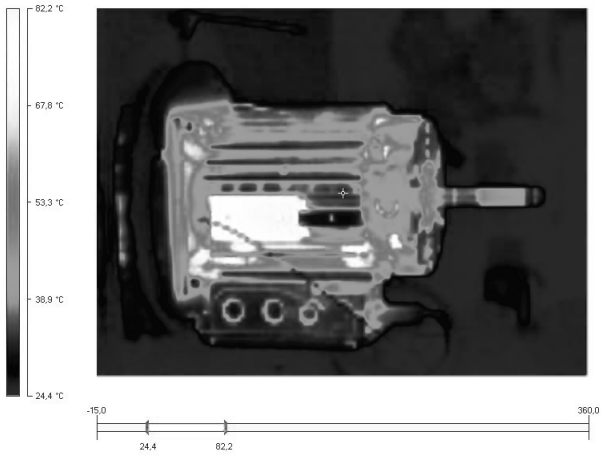

Figure 12. Picture of the thermal imaging camera.

	measured	simulated
frame	101	102
stator sheet - slot insulation (pos. 1)	139	138
slot insulation - copper (pos. 2)	146	147
inside copper (pos. 3)	151	147
stator teeth (pos. 4)	135	139
rotor surface	120	117

Table I
COMPARISON OF MEASURED AND SIMULATED TEMPERATURES.

thermal conductivities, used for the numerical simulation, are shown in table II. The slot insulation causes a temperature decline from 146^oC on the copper side to 139^oC on the stator sheet side. Setting the heat flow coefficient for the thin layer boundary condition to $30\frac{\mathrm{W}}{\mathrm{m^2K}}$ achieves this temperature decline in the simulation. Comparing the temperatures between

Material	Thermal conductivity $\left[\frac{\mathrm{W}}{\mathrm{mK}}\right]$
Aluminium (Frame)	230
Lamination Sheet	15
Copper	380
Air	$0,0024$

Table II
USED THERMAL CONDUCTIVITIES.

stator and rotor yield a temperature difference of 15^oC. In the simulation this difference can be achieved by adapting the heat flow coefficient of the air gap boundary condition to $1,82\frac{\mathrm{W}}{\mathrm{m^2K}}$. Finally a result of the thermal imaging camera, showing the temperature distribution on the frame is illustrated in fig. 12.

V. CONCLUSIONS

In this paper a thermal finite element solver is introduced using boundary conditions to take slot insulation and the air gap into account. Thereby, the computation time can be reduced significantly. The values for the heat flow coefficients, necessary to parametrize the boundary conditions, are determined by measurements. By use of this adapted heat flow coefficients, very accurate simulation results can be achieved. In future studies, the applied heat flow coefficients and thermal conductivities need to be validated with new machines.

REFERENCES

[1] A. M. EL-Refaie, N. C. Harris, T. M. Jahns, and K. M. Rahman, "Thermal Analysis of Multibarrier Interior PM Synchronous Machine Using Lumped Parameter Model," *IEEE Transactions on Energy Conversion*, vol. 19, no. 2, pp. 303–309, 2004.

[2] A. Boglietti, A. Cavagnino, and D. Staton, "Determination of Critical Parameters in Electrical Machine Thermal Models," *IEEE Industry Application Conference, 42nd IAS Annual Meeting*, pp. 73–80, 2007.

[3] P. H. Mellor, D. Roberts, and D. R. Turner, "Lumped parameter thermal model for electrical machines of TEFC design," *IEE Proceedings Electric Power Application*, vol. 138, no. 5, pp. 205–218, 1991.

[4] S. S. Rao, *The Finite Element Method in Engineering*. Burlington: Elsevier Butterworth–Heinemann, vierte ed., 2005.

[5] J. Driesen, R. Belmanns, and K. Hameyer, "Finite element modelling of thermal contact resistances and insulation layers in electrical machines," *IEEE Transactions on Industry Applications*, vol. 37, no. 1, pp. 15–20, 2001.

[6] J. H. Lienhard, *A Heat Transfer Textbook*. New Jersey: Prentice Hall, Inc., zweite ed., 1987.

[7] G. I. Taylor, "Stability of a viscous fluid contained between two rotating cylinders," *Philosophical Transactions of the Royal Society of London, series A*, vol. 223, pp. 289–343, 1923.

[8] K. M. Becker and J. Kaye, "The influence of a radial temperature gradient on the instability of fluid flow in an annulus with an inner rotating cylinder," *Trans. of the ASME, Journ. of Heat Transfer*, vol. 84, pp. 106–110, May 1962.

[9] K. M. Becker and J. Kaye, "Measurement of diabatic flow in an annulus with inner rotating cylinder," *Trans. of the ASME, Journ. of Heat Transfer*, vol. 84, pp. 97–105, May 1962.

[10] C. Gazley Jr., "Heat–transfer characteristics of the rotational and axial flow between conectric cylinders," *Trans. of the ASME*, vol. 80, pp. 79–90, 1958.

[11] Y. Bertin, E. Videcoq, S. Thieblin, and D. Petit, "Thermal behavior of an electrical motor through a reduced model," *IEEE Transactions on Energy Conversion*, vol. 15, pp. 129–134, June 2000.

[12] O. C. Zienkiewicz and R. L. Taylor, *The finite element method*, vol. 2. McGRAW–Hill Book Company (UK) Limited, vierte ed., 1991.